short communications

Pseudo-merohedral twinning in monoclinic crystals of human orotidine-5′-monophosphate decarboxylase

**Julia G. Wittmann and
Markus G. Rudolph***

Department of Molecular Structural Biology,
Justus-von-Liebig-Weg 11, 37077 Göttingen,
Germany

Correspondence e-mail:
markus.rudolph@bio.uni-goettingen.de

Human UMP synthase is a bifunctional enzyme that catalyzes the penultimate and last steps in the *de novo* biosynthesis of UMP. In contrast to prokaryotes, UMP synthase from higher eukaryotes combines the orotate phosphoribosyl-transferase and the orotidine-5′-monophosphate (OMP) decarboxylase activities on a single polypeptide chain. The decarboxylase activity is unusual in that it represents the fastest rate acceleration of any enzyme studied to date. Although several crystal structures of OMP decarboxylases have been described, the precise decarboxylation mechanism remains elusive. The crystal structure of the OMP decarboxylase domain from human UMP synthase was determined by molecular replacement using data from a highly twinned monoclinic crystal. The space group is $P2_1$, with unit-cell parameters $a = 69.18$, $b = 61.70$, $c = 69.17$ Å, $\beta = 113.06°$. Self-rotation function analysis and various intensity statistics revealed the presence of pseudo-merohedral twinning, but these tests underestimated the true twin fraction of $\alpha \simeq 0.44$. Data analysis, the origin of the twinning and structure determination are discussed.

1. Introduction

Orotidine-5′-monophosphate decarboxylase (OMPD) catalyzes the last step in *de novo* pyrimidine biosynthesis, the decarboxylation of orotidine-5′-monophosphate (OMP) to UMP. In contrast to other decarboxylases, this reaction does not require any cofactor or metal ion such as thiamine pyrophosphate or Zn^{2+}. OMPD is a remarkable enzyme because it displays the largest known rate acceleration of any catalyzed reaction described so far. The half-time of the spontaneous decarboxylation of OMP to UMP has been estimated to be 78 million years. In contrast, the yeast enzyme converts OMP to UMP with a half-life of 18 ms, an effective acceleration of 10^{17}. Despite in-depth enzymology and several crystal structures of OMPD both in the apo form and bound to substrates, products and inhibitors, the precise enzymatic mechanism remains elusive (Miller & Wolfenden, 2002). Human OMPD is the C-terminal part of the UMP synthase enzyme. It is fused to orotate phosphoribosyltransferase, which catalyzes the penultimate step of *de novo* pyrimidine biosynthesis. As such, the human UMP synthase enzyme may be a potential cancer drug target, similar to AICAR transformylase, which also possesses the final two activities for *de novo* purine biosynthesis (Greasley *et al.*, 2001).

We have cloned, purified and crystallized the C-terminal domain of human UMP synthase harbouring the OMPD activity. Unfortunately, crystals of OMPD exhibited a high degree of pseudo-hemihedral twinning; however, this did not hamper structure determination. In this study, we outline the analysis and phasing of the OMPD diffraction data from pseudo-merohedrally twinned crystals using molecular replacement.

When two or more crystals intergrow in different relative orientations to form a larger aggregate, a twinned crystal results (Catti & Ferraris, 1976; Donnay & Donnay, 1974; Friedel, 1926). Should the crystal lattices overlap in two dimensions, an epitaxic twin is present. A distinct lattice for each twin can then be observed in the diffraction pattern and the lattice for a single twin can often be extracted. In contrast, merohedral twins are characterized by a three-dimensional intergrowth of crystals and produce a single diffraction pattern which does not reveal the presence of twinning *per se* (Yeates, 1997; Yeates
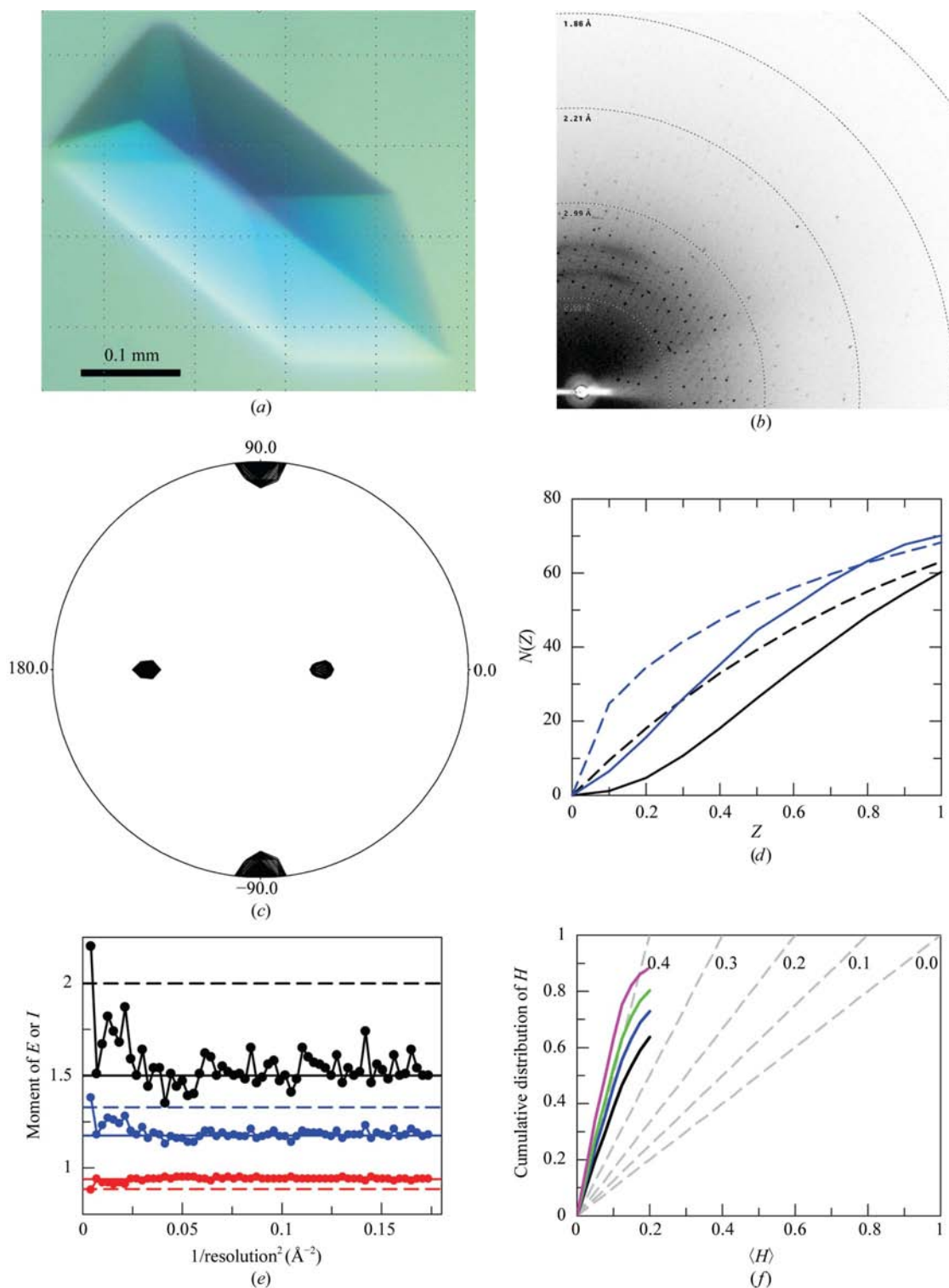
Figure 1
Detection and analysis of twinning. (*a*) Crystal of OMPD. (*b*) Diffraction pattern of twinned monoclinic OMPD collected on a rotating-anode generator. (*c*) Stereographic projection plot of the $\kappa = 180°$ section of the self-rotation function of the twinned native data set. The function was calculated with resolution limits of 15 and 5 Å and a Patterson integration radius of 23 Å and was contoured at >40% of the maximum peak height using *POLARRFN* (Collaborative Computational Project, Number 4, 1994). The data were reduced in *P*2 and the plot shows a twofold axis ($\omega = 33.4$, $\varphi = 0.0°$) with a height of 66% of the origin peak ($\omega = 90.0$, $\varphi = 90.0°$) perpendicular to the *b* axis. The NCS axis gives rise to another axis ($\omega = 54.6$, $\varphi = 180.0°$) that is perpendicular to the first two and completes the pseudo-orthorhombic setting. (*d*) Cumulative distribution of $Z = I/\langle I \rangle$, where I is the intensity, for the acentric (continuous black line) and centric (continuous blue line) OMPD data. The theoretical distributions for untwinned data are shown as dashed lines. The sigmoidal shape of the distribution of the acentric reflections indicates twinning. (*e*) Resolution-dependence of the first (red) and third (blue) moments on E and the second moment on I (black). Dashed and continuous lines indicate the expected values for untwinned and perfectly twinned data, respectively. The high-resolution cutoff for the calculations in (*d*) and (*e*) was 2.4 Å. (*f*) Estimation of the twin fraction α by plotting the cumulative fractional intensity difference of acentric twin-related intensities, $H = |I_1 - I_2|/(I_1 + I_2)$, as a function of H (Yeates, 1988). The initial slope of the distribution is a measure of α. Colours correspond to different resolution cutoffs (black, 1.85 Å; blue, 2.2 Å; green, 2.5 Å; magenta, 3.5 Å). The dashed lines represent the expected slopes for the indicated twin fractions.

Table 1
Crystallographic data collection and analysis.

	$P2_1$	$C222_1$
Wavelength (Å)	1.5419	1.5419
Resolution range† (Å)	[50–4.0] 50–1.85 (1.92–1.85)	[50–4.0] 50–1.85 (1.92–1.85)
Unique reflections†	[4447] 44425 (3916)	[2505] 23501 (2165)
Rejected reflections	1615 (1.4%)	6265 (5.5%)
Completeness† (%)	[94.1] 96.8 (85.5)	[99.2] 99.1 (92.8)
R_{sym}†‡ (%)	[3.4] 7.8 (41.1)	[5.9] 11.6 (47.8)
$R_{r.i.m.}$†§ (%)	[4.2] 9.8 (52.8)	[8.4] 13.6 (55.2)
Average $I/\sigma(I)$†	[27.0] 11.5 (1.9)	[22.1] 12.6 (2.3)
Multiplicity of observations†	[2.8] 2.6 (2.1)	[4.8] 4.9 (3.8)
Mosaicity (°)	0.82	0.82
Mean $|E^2 - 1|$¶	0.559 (0.736)	0.541
$\langle|I|^2\rangle/\langle|I|\rangle^2$††	1.7 (2.0/1.5)††	n.a.
$\langle|F|\rangle^2/\langle|F|^2\rangle$††	0.866 (0.785/0.865)	n.a.

† Values in parentheses and square brackets refer to the highest and lowest resolution shells, respectively. ‡ $R_{sym} = 100 \times \sum_{hkl}\sum_i |I_{hkl} - \langle I_{hkl}\rangle|/\sum_{hkl}\sum_i I_{hkl}$. § $R_{r.i.m.} = 100 \times \sum_h [N/(N-1)]^{1/2} \sum_i |I_i(h) - \langle I(h)\rangle|/\sum_h \sum_i I_i(h)$, where N is the multiplicity. ¶ The value in parentheses is the expected value for untwinned data. †† Values in parentheses are the expected values for untwinned/perfectly twinned data. n.a., not analyzed.

& Fam, 1999). Hemihedrally and tetartohedrally twinned crystals are composed of two and four different twin domains, respectively (Chandra *et al.*, 1999; Yeates, 1997; Yeates & Fam, 1999), which all contribute to generate a superposed diffraction pattern (Liang *et al.*, 1996; Lietzke *et al.*, 1996). Twinned crystals are described by the twin operator relating the twin domains and the twin fraction(s) α, *i.e.* the fractional volume(s) of the individual twin domains.

In merohedral twins, the twinning operator introduces additional symmetry that is a symmetry operator of the apparent higher symmetry Laue group of the same crystal system. Thus, hemihedral twinning is observed in the tetragonal, trigonal, hexagonal and cubic crystal systems, while tetartohedral twinning can occur in trigonal crystals (Barends *et al.*, 2005; Rosendal *et al.*, 2004). In pseudo-merohedral twins, the twin operator belongs to a higher Laue symmetry than possible for the crystal system of the sample. Examples of this rare type of twinning are orthorhombic crystals that emulate tetragonal symmetry (Adams *et al.*, 2006), primitive monoclinic crystals that emulate primitive orthorhombic (Larsen *et al.*, 2002) or C-centred orthorhombic symmetry (Barends & Dijkstra, 2003; Mueller, Muller *et al.*, 1999; Rudolph *et al.*, 2004), or C-centred monoclinic crystals that emulate face-centred orthorhombic symmetry (Lehtiö *et al.*, 2005).

The successful use of twinned data for structure determination of macromolecules by molecular replacement (Breyer *et al.*, 1999; Contreras-Martel *et al.*, 2001; Larsen *et al.*, 2002; Luecke *et al.*, 1998; Rabijns *et al.*, 2001; Redinbo & Yeates, 1993; Taylor *et al.*, 2000; Trame & McKay, 2001), single or multiple isomorphous replacement (Ban *et al.*, 1999; Declercq & Evrard, 2001; Forst *et al.*, 1998; Goldman *et al.*, 1987; Hillig *et al.*, 1999; Mueller, Muller *et al.*, 1999; Mueller, Schubel *et al.*, 1999; Terwisscha van Scheltinga *et al.*, 2001) and multiple anomalous dispersion (Barends *et al.*, 2005; Rudolph *et al.*, 2003; Yang *et al.*, 2000) shows that twinning may complicate phasing and refinement, but does not render it impossible.

2. Materials and methods

2.1. Protein purification, crystallization and data collection

The coding region for the orotidine-5'-phosphate decarboxylase domain of human UMP synthase (Swiss-Prot entry P11172) was amplified from a cDNA library using primers 5'-GGCCCATGG-AACTCAGCTTCGGTGCACGTG-3' and 5'-GGAATTCTCAAA-CACCAAGTCTACTCAAATACGCTT-3' and cloned into the

NcoI/EcoRI sites of pETM-30 (G. Stier, EMBL Heidelberg). This expression vector allows the production of an N-terminally His$_6$-tagged glutathione-S-transferase (GST) fusion protein containing a tobacco etch virus (TEV) protease site between His$_6$-GST and the target protein. The His$_6$-GST-OMPD fusion protein was produced overnight at 303 K in *E. coli* Rosetta2 (DE3) cells after induction with 0.1 mM IPTG at an OD_{600} of 0.6. Cells were harvested, resuspended in 50 mM Tris–HCl, 100 mM NaCl pH 7.5 and disrupted in a fluidizer (Microfluidics Corp., Newton, MA, USA). After centrifugation, the GST-OMPD fusion protein was bound to a glutathione Sepharose column, eluted with the same buffer containing 20 mM reduced glutathione and hydrolyzed with His$_6$-tagged TEV protease at 277 K for 2–3 d. His$_6$-tagged proteins were separated from OMPD by Ni^{2+}–NTA affinity chromatography. The flowthrough containing OMPD (residues 224–480 of human UMP synthase preceded by a vector-derived GAM sequence) was concentrated and applied onto an S200 size-exclusion column (Amersham) equilibrated in 20 mM HEPES–NaOH pH 7.4. OMPD was concentrated by ultrafiltration to 5 mg ml^{-1} and stored at 193 K.

5 mg ml^{-1} OMPD in 20 mM HEPES–NaOH pH 7.4 was crystallized in a sitting-drop setup by mixing it with 0.1 M Tris–HCl pH 8.0, 1.8 M $(NH_4)_2SO_4$ in a 1:1 ratio at 295 K (Fig. 1a). Crystals were cryoprotected with 20%(*v/v*) glycerol in mother liquor and flash-cooled in liquid nitrogen. A data set was collected to 1.85 Å resolution (Fig. 1b; Table 1) in-house from a cryocooled single crystal at 128 K. Data reduction was performed using the *HKL* package (Otwinowski & Minor, 1997). Indexing and integration were possible in both primitive monoclinic (*P*2) and C-centred orthorhombic (*C*222) settings, leading to unit-cell parameters of $a = 69.18$, $b = 61.70$, $c = 69.17$ Å, $\beta = 113.06°$ and $a = 76.30$, $b = 115.41$, $c = 61.70$ Å, respectively.

2.2. Data analysis

The presence of a twofold screw axis was established by analysis of the systematic absences from data processed in *P*2, leaving $P2_1$ and $C222_1$ (a minimal non-isomorphic supergroup of $P2_1$) as possible space groups. Self-rotation function analysis of the data processed in *P*2 using *POLARRFN* (Collaborative Computational Project, Number 4, 1994) with resolution limits of 10–5 Å and a Patterson integration radius of 23 Å showed the presence of twofold axes perpendicular to the crystallographic *b* axis, indicating possible higher (orthorhombic) space-group symmetry or the presence of a NCS axis perpendicular to, but not necessarily intersecting, the unique *b* axis. As discussed below, the true space group is $P2_1$ and the presence of a noncrystallographic (NCS) axis perpendicular to the crystallographic twofold together with the fortuitous unit-cell parameters $a \simeq c$ allows twinning and emulates orthorhombic symmetry.

3. Results and discussion

3.1. Detection of twinning in crystals of OMPD

Fortuitous unit-cell parameters in monoclinic crystals occur often (see below) and may give rise to twinning in several ways. If $\beta \simeq 90°$, a primitive orthorhombic crystal system may be emulated (Larsen *et al.*, 2002). The twin law in this case is $h, -k, -l$ or $-h, -k, l$, reflecting twofold twinning about the *a* or *c* axes, respectively. A less common type of pseudo-merohedral twinning in the monoclinic system may occur if the relation $c\cos\beta = -a/2$ holds, *i.e.* the two unit cells of the twin domains share the same *a* and *b* axes but with opposite directions. The corresponding twin law is $-h, -k, h + l$ and describes a twofold rotation about an axis perpendicular to the *a* and *b* axes (*i.e.*

along c^*). Diffraction patterns from these crystals may be indexed in a C-centred orthorhombic symmetry (Declercq & Evrard, 2001; Rudolph *et al.*, 2004). Finally, if the unit-cell parameters are $a \simeq c$, the unit cell may be rotated about the ac plane diagonal for a complete superposition of the unit cells, giving rise to twinning according to the law $l, -k, h$. It should be noted that the program *TRUNCATE* (Collaborative Computational Project, Number 4, 1994) reports a possible twinning warning for all of these cell settings.

Warning signs for twinning have been compiled (Herbst-Irmer & Sheldrick, 1998) and include apparent higher symmetry arising from the twin operator, which introduces additional symmetry that is not part of the Laue symmetry of the space group. The first indication of possible partial hemihedral twinning in OMPD crystals was the observation that the data could be indexed, processed and scaled in both $P2_1$ and $C222_1$ with reasonable overall R_{sym} values (Table 1). Calculation of the packing density assuming two and one molecule(s) in the $P2_1$ and $C222_1$ asymmetric units, respectively, yielded a Matthews coefficient (V_M; Matthews, 1968) of 2.1 Å^3 Da^{-1} (40% solvent content) for both cases. In the $C222_1$ setting, the volume of the asymmetric unit is only half that of the $P2_1$ unit cell, leaving the packing density unchanged if one molecule per $C222_1$ asymmetric unit is assumed. Thus, packing-density considerations did not provide obvious indications of twinning. However, resolution-dependent inspection of R_{sym} revealed considerable differences in data reduction between the two space groups (Table 1). This difference is even more pronounced when the redundancy-independent merging R values ($R_{r.i.m.}$; Weiss, 2001) are compared: the values for the low-resolution shell differ by a factor of two (1.7 for R_{sym}). In contrast, comparison of the R_{sym} or $R_{r.i.m.}$ values for the high-resolution shells seems less informative as the values for the two crystal settings are very similar. In addition, while in $P2_1$ a total of 1.4% of reflections were rejected during scaling, this number increased to 5.5% when scaling was performed in $C222_1$. Thus, the true symmetry is monoclinic rather than orthorhombic.

Further analysis of the diffraction data using *XPREP* (Bruker AXS) revealed a lower mean $|E^2 - 1|$ value of 0.575 for the OMPD data set than expected for noncentrosymmetric space groups (0.736; Table 1), which represents another hallmark of twinning (Herbst-Irmer & Sheldrick, 1998). The presence of pseudo-222 symmetry is apparent from a self-rotation function analysis of the data that were reduced in $P2$ (Fig. 1c). The $\kappa = 180°$ section shows twofold axes perpendicular to the crystallographic twofold axis. A further indication of the presence of hemihedral twinning is an abnormal distribution of $Z = I/\langle I \rangle$. The cumulative intensity distribution of the OMPD data, as calculated using *TRUNCATE* (Collaborative Computational Project, Number 4, 1994), is sigmoidal in shape compared with the expected distribution of untwinned data (Fig. 1d), further pointing to twinned crystals. Only few possibilities exist for a monoclinic system to become twinned and thus to emulate an orthorhombic metric (see above). A relatively common situation seems to be a monoclinic cell with $a \simeq c$ (Yang *et al.*, 2000), which applies to the OMPD data.

To assess the twin fraction of the OMPD data, different twinning tests were employed (Kahlenberg, 1999) using the programs *CNS* (Brünger *et al.*, 1998) and *DETWIN* (Collaborative Computational Project, Number 4, 1994). For acentric untwinned data, the second moment, *i.e.* the expected ratio of the average-squared intensity to the square of the average intensities ($\langle I^2 \rangle / \langle |I| \rangle^2$), is 2; for perfectly twinned data, it is 1.5. The OMPD data set value was 1.7, suggesting twinning with a high twin fraction. Similarly, the first and third moments of E also indicated the presence of twinning (Fig. 1e). As partial twinning tests in point group 2 with the presence of pseudo-

merohedral twinning are not supported by *CNS*, *XPREP* or the twinning server (Yeates, 1997), the twin fraction was assessed with *DETWIN* (Collaborative Computational Project, Number 4, 1994) using the cumulative distribution of H (Yeates, 1988), where $H = |I_{obs1} - I_{obs2}|/(I_{obs1} + I_{obs2})$. The twin law $l, -k, h$ describes a real-space rotation about an axis perpendicular to the crystallographic twofold in the ac plane. Calculation of the H function using this twin law yielded twin-fraction estimates of 0.35–0.42 depending on the resolution of the data used for the calculation (Fig. 1f). These values are similar to the twin fraction of 0.38 estimated from the Britton plot (Fisher & Sweet, 1980) (not shown).

The estimates from both intensity statistics are lower than the true twin fraction (0.44) as inferred by initial atomic refinement in *SHELXL* (Sheldrick & Schneider, 1997). Two possible explanations, pointed out by reviewers, might account for this discrepancy. Measurement errors in the observed data may increase the differences between the twin-related reflections, resulting in lower calculated twin fractions. In addition, the assumption of the intensity statistics that the twin-related reflections are independent may not hold in the OMPD case. The NCS axis does not intersect the crystallographic b axis or the true space group would be $C222_1$ (see below). As the NCS axis almost exactly describes a $C222_1$ symmetry element, the twin operator relates 'almost symmetry-equivalent' reflections of similar intensities, leading to a bias in the intensity statistics that is more severe the closer the NCS axis approaches true $C222_1$ symmetry. The effect of the twin operator in averaging the reflection intensities would then be less pronounced, leading in turn to the observed underestimation of the twin fraction from intensity statistics. The resolution-dependent calculation of the H function (Fig. 1f) also reveals that the underestimation of the twin fraction is stronger when higher resolution data are included, although the effects of pseudo-symmetry on the intensity distributions should be less dominant at lower resolution. The OMPD data point to a greater influence of measurement errors on the uncertainty of the twin-fraction estimation, but whether this observation holds for other pseudo-merohedral twins remains to be investigated.

3.2. Structure determination using twinned data

The $\kappa = 180°$ section of the self-rotation function in $P2$ showed strong twofold-symmetry elements perpendicular to the crystallographic twofold. As no translational information is present in a self-rotation function, the additional twofolds may or may not intersect with each other. In the first case this could lead to true crystallographic symmetry in an orthorhombic setting, while in the second case the additional symmetry would be local. In the OMPD data, a twofold axis runs perpendicular to the b axis and in the ac plane (Fig. 2a). Rotation of the monoclinic cell about this axis switches the crystallographic a and c axes and inverts the b-axis direction, leading to the twin law $l, -k, h$. In addition, the two perpendicular axes generate a third axis which is perpendicular to the first two twofolds. Thus, the additional symmetry element emulates an orthorhombic unit cell (dashed line in Fig. 2a), indicating that the NCS rotation can promote the twinning rotation, as has been found in a statistical analysis of the PDB (Lebedev *et al.*, 2006). Indeed, both peaks in the $\kappa = 180°$ self-rotation function are equivalent choices for the NCS axis and the twin element. However, it should be noted that the presence of a twofold NCS axis perpendicular to the crystallographic twofold in the monoclinic setting does not necessarily lead to a twinned crystal (Kefala & Weiss, 2006).

Molecular replacement was performed in space group $P2_1$ using the untreated twinned data. A previously determined human OMPD
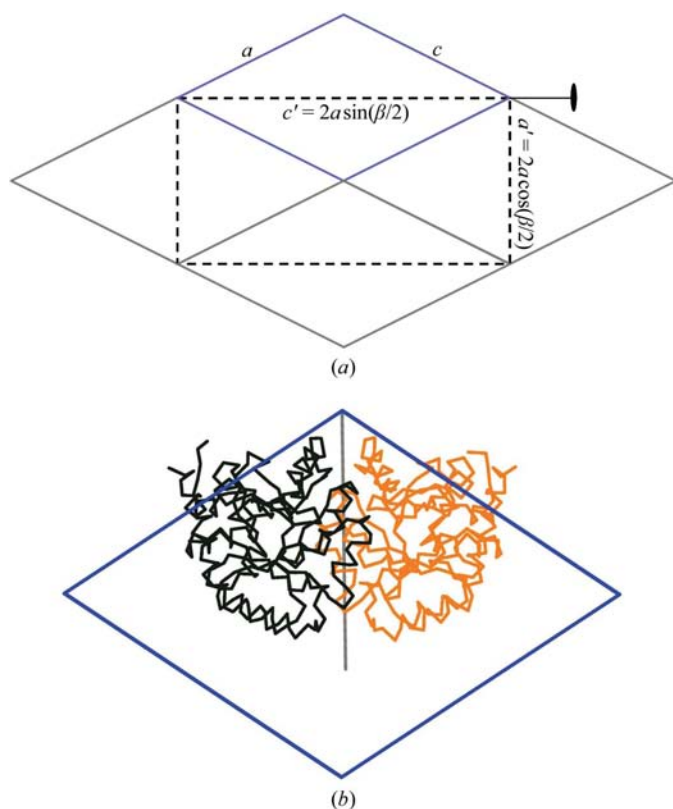
Figure 2
Geometric characteristics of the monoclinic OMPD crystal. (*a*) Arrangement of the $P2_1$ cell to allow twinning and emulation of the $C222_1$ cell. The unit cell (blue) is projected along the *b* axis. A 180° rotation of the monoclinic cell about an axis perpendicular to the *b* axis in the *ac* plane leads to complete superposition of the two primitive lattices according to the real-space relation $b' = 2a\sin(\beta/2)$. Additional primitive unit cells are drawn in grey. The effect of the twin operator is to exchange the *a* and *c* axes and invert the *b*-axis direction. According to the twin law $l, -k, h$ pseudo-centring is emulated and the resulting $C222_1$ cell ($a' = 76.3$, $b' = 115.4$ Å) is indicated as a dashed line. (*b*) The two molecules in the asymmetric unit are shown as C^α traces, with the unit cell projected along the *b* axis as in (*a*). Each OMPD monomer is coloured individually and the NCS axis is indicated as a grey line. As the NCS axis is perpendicular to the *b* axis, a third twofold axis is emulated. Thus, there are two choices for the twin element.

structure (to be published) was used as the search model in *Phaser* (Collaborative Computational Project, Number 4, 1994) or *COMO* (Jogl *et al.*, 2001) and yielded two clear rotation solutions, which were related by a 180° rotation in accord with the presence of twofold NCS. The packing-evaluation functions in *Phaser* and *COMO* were needed to eliminate all translation solutions that placed the two molecules in different twin domains. Since the packing functions are so computationally effective, it was not tested whether detwinning of the data for structure-determination purposes gave higher signal-to-noise ratios or a larger number of correct solutions.

OMPD is a dimer in solution and also in the $P2_1$ crystal, where the two molecules in the asymmetric unit are related by a twofold rotation (Fig. 2*b*) followed by a translation of <1 Å. The NCS axis of the OMPD dimer is perpendicular to the crystallographic twofold and almost intersects it (distance 0.5 Å). The geometry of the asymmetric unit allows the twinning, but slight rigid-body motions of the OMPD monomers can result in the NCS axis becoming crystallographic, with the true space group then being $C222_1$ and no pseudo-symmetry being present. In this case, the asymmetric unit contains only half of the biological OMPD dimer. The crystal habit does not indicate the crystal system, but it seems that ligands such as UMP can induce asymmetry in the OMPD dimer (data not shown).

4. Conclusions

The refined twin fraction of 0.44 for the OMPD data is close to perfect twinning, but resolution-dependent inspection of R_{sym} for data reduction in both $P2_1$ and $C222_1$ space groups could still easily resolve the true symmetry as monoclinic. Recently, a survey of the PDB for twinned data where twinning may have been overlooked during structure refinement was performed and concluded that this was likely for 78 structures (Lebedev *et al.*, 2006). Among these, 12 were in space group $P2_1$. Because twinning in the monoclinic crystal system is expected to be less frequent than in the tetragonal, trigonal, hexagonal and cubic systems, the question arose as to how often monoclinic crystals grow with unit-cell parameters that in principle allow twinning. A search of the April 2007 PDB for possible monoclinic twins similar to OMPD revealed several cases where twinning may be present in the data. The unit-cell parameters of 5174 entries with space group $P2_1$ (including redundant structures such as mutants and ligand complexes) were tested to determine whether they fulfilled the relation $0.98 < a/c < 1.02$. Of the 430 structures whose unit-cell parameters fulfilled this condition, 56 and 27, respectively, had β angles of 120 ± 1 or $90 \pm 1°$, and were disregarded as they may emulate hexagonal or tetragonal metrics. 347 structures, *i.e.* ∼7% of all structures in $P2_1$, remained with unit-cell parameters that could allow twinning. Of the 232 data sets that were available for analysis, 25 had an $|E^2 - 1|$ value of ≤0.67 as determined by *XPREP*, which could indicate twinning. This was corroborated for 22 structures by a sigmoidal cumulative intensity distribution of the acentric reflections as calculated by *TRUNCATE* (Collaborative Computational Project, Number 4, 1994), suggesting the presence of twinning in these data sets. No further analysis as to whether twinning was accounted for during refinement was performed. In summary, this type of pseudo-merohedral twinning seems to be relatively common in monoclinic crystals of macromolecules.

References

Adams, J. J., Anderson, B. F., Norris, G. E., Creamer, L. K. & Jameson, G. B. (2006). *J. Struct. Biol.* **154**, 246–254.
Ban, N., Nissen, P., Hansen, J., Capel, M., Moore, P. B. & Steitz, T. A. (1999). *Nature (London)*, **400**, 841–847.
Barends, T. R., de Jong, R. M., van Straaten, K. E., Thunnissen, A. M. & Dijkstra, B. W. (2005). *Acta Cryst.* D**61**, 613–621.
Barends, T. R. & Dijkstra, B. W. (2003). *Acta Cryst.* D**59**, 2237–2241.
Breyer, W. A., Kingston, R. L., Anderson, B. F. & Baker, E. N. (1999). *Acta Cryst.* D**55**, 129–138.
Brünger, A. T., Adams, P. D., Clore, G. M., DeLano, W. L., Gros, P., Grosse-Kunstleve, R. W., Jiang, J.-S., Kuszewski, J., Nilges, M., Pannu, N. S., Read, R. J., Rice, L. M., Simonson, T. & Warren, G. L. (1998). *Acta Cryst.* D**54**, 905–921.
Catti, M. & Ferraris, G. (1976). *Acta Cryst.* A**32**, 163–165.
Chandra, N., Acharya, K. R. & Moody, P. C. (1999). *Acta Cryst.* D**55**, 1750–1758.
Collaborative Computational Project, Number 4 (1994). *Acta Cryst.* D**50**, 760–763.
Contreras-Martel, C., Martinez-Oyanedel, J., Bunster, M., Legrand, P., Piras, C., Vernede, X. & Fontecilla-Camps, J. C. (2001). *Acta Cryst.* D**57**, 52–60.
Declercq, J. P. & Evrard, C. (2001). *Acta Cryst.* D**57**, 1829–1835.
Donnay, G. & Donnay, J. D. H. (1974). *Can. Mineral.* **12**, 422–425.
Fisher, R. G. & Sweet, R. M. (1980). *Acta Cryst.* A**36**, 755–760.
Forst, D., Welte, W., Wacker, T. & Diederichs, K. (1998). *Nature Struct. Biol.* **5**, 37–46.

Friedel, G. (1926). *Leçons de Cristallographie.* Nancy/Paris/Strasbourg: Berger-Leurault.

Goldman, A., Ollis, D. L. & Steitz, T. A. (1987). *J. Mol. Biol.* **194**, 143–153.

Greasley, S. E., Horton, P., Ramcharan, J., Beardsley, G. P., Benkovic, S. J. & Wilson, I. A. (2001). *Nature Struct. Biol.* **8**, 402–406.

Herbst-Irmer, R. & Sheldrick, G. M. (1998). *Acta Cryst.* B**54**, 443–449.

Hillig, R. C., Renault, L., Vetter, I. R., Drell, T. I., Wittinghofer, A. & Becker, J. (1999). *Mol. Cell,* **3**, 781–791.

Jogl, G., Tao, X., Xu, Y. & Tong, L. (2001). *Acta Cryst.* D**57**, 1127–1134.

Kahlenberg, V. V. (1999). *Acta Cryst.* B**55**, 745–751.

Kefala, G. & Weiss, M. S. (2006). *Acta Cryst.* F**62**, 1116–1119.

Larsen, N. A., Heine, A., de Prada, P., el Redwan, R., Yeates, T. O., Landry, D. W. & Wilson, I. A. (2002). *Acta Cryst.* D**58**, 2055–2059.

Lebedev, A. A., Vagin, A. A. & Murshudov, G. N. (2006). *Acta Cryst.* D**62**, 83–95.

Lehtiö, L., Fabrichniy, I., Hansen, T., Schönheit, P. & Goldman, A. (2005). *Acta Cryst.* D**61**, 350–354.

Liang, J., Ealick, S., Nielsen, S., Schreiber, S. L. & Clardy, J. (1996). *Acta Cryst.* D**52**, 207–210.

Lietzke, S. E., Carperos, V. E. & Kundrot, C. E. (1996). *Acta Cryst.* D**52**, 687–692.

Luecke, H., Richter, H. T. & Lanyi, J. K. (1998). *Science,* **280**, 1934–1937.

Matthews, B. W. (1968). *J. Mol. Biol.* **33**, 491–497.

Miller, B. G. & Wolfenden, R. (2002). *Annu. Rev. Biochem.* **71**, 847–885.

Mueller, U., Muller, Y. A., Herbst-Irmer, R., Sprinzl, M. & Heinemann, U. (1999). *Acta Cryst.* D**55**, 1405–1413.

Mueller, U., Schubel, H., Sprinzl, M. & Heinemann, U. (1999). *RNA,* **5**, 670–677.

Otwinowski, Z. & Minor, W. (1997). *Methods Enzymol.* **276**, 307–326.

Rabijns, A., Verboven, C., Novoa de Armas, H., Van Damme, E. J., Peumans, W. J. & De Ranter, C. J. (2001). *Acta Cryst.* D**57**, 609–611.

Redinbo, M. R. & Yeates, T. O. (1993). *Acta Cryst.* D**49**, 375–380.

Rosendal, K. R., Sinning, I. & Wild, K. (2004). *Acta Cryst.* D**60**, 140–143.

Rudolph, M. G., Kelker, M. S., Schneider, T. R., Yeates, T. O., Oseroff, V., Heidary, D. K., Jennings, P. A. & Wilson, I. A. (2003). *Acta Cryst.* D**59**, 290–298.

Rudolph, M. G., Wingren, C., Crowley, M. P., Chien, Y. H. & Wilson, I. A. (2004). *Acta Cryst.* D**60**, 656–664.

Sheldrick, G. M. & Schneider, T. R. (1997). *Methods Enzymol.* **277**, 319–343.

Taylor, H. O., O'Reilly, M., Leslie, A. G. & Rhodes, D. (2000). *J. Mol. Biol.* **303**, 693–707.

Terwisscha van Scheltinga, A. C., Valegard, K., Ramaswamy, S., Hajdu, J. & Andersson, I. (2001). *Acta Cryst.* D**57**, 1776–1785.

Trame, C. B. & McKay, D. B. (2001). *Acta Cryst.* D**57**, 1079–1090.

Weiss, M. S. (2001). *J. Appl. Cryst.* **34**, 130–135.

Yang, F., Dauter, Z. & Wlodawer, A. (2000). *Acta Cryst.* D**56**, 959–964.

Yeates, T. O. (1997). *Methods Enzymol.* **276**, 344–358.

Yeates, T. O. (1988). *Acta Cryst.* A**44**, 142–144.

Yeates, T. O. & Fam, B. C. (1999). *Structure Fold. Des.* **7**, R25–R29.